ABSTRACT

Title of Thesis: DECODING OF WALKING KINEMATICS FROM NON-INVASIVELY ACQUIRED ELECTROENCEPHALOGRAPHIC SIGNALS IN STROKE PATIENTS

Kevin Christopher Nathan, Master of Science, 2012

Thesis directed by: Professor Jose Luis Contreras-Vidal,

Department of Electrical and Computer Engineering, University of Houston, Houston, TX

Visiting Professor, Department of Kinesiology, University of Maryland, College Park, MD

Our group has recently shown the feasibility of decoding kinematics of controlled walking from the lower frequency range of electroencephalographic (EEG) signals during a precision walking task. Here, we turn our attention to stroke survivors who have had lesions resulting in hemiparetic gait. We recorded the EEG of stroke recovery patients during a precision treadmill walking task while tracking bilaterally the kinematics of the hips, knees, and ankles. In offline analyses, we applied a Wiener Filter and two unscented Kalman filters of 1^{st} and 10^{th} orders to predict estimates of the kinematic parameters from scalp EEG. Decoding accuracies from four patients who have had cortical and subcortical strokes were comparable with previous studies in healthy subjects. With improved decoding of EEG signals from damaged brains, we hope we can soon correlate activity to more intentional and normal-form walking that can guide users of a powered lower-body prosthetic or exoskeleton.

MASTER'S THESIS:

DECODING OF WALKING KINEMATICS FROM NON-INVASIVELY ACQUIRED ELECTROENCEPHALOGRAPHIC SIGNALS IN STROKE PATIENTS

Submitted by:

Kevin Christopher Nathan

Thesis submitted to the Faculty of the Graduate School of the
University of Maryland, College Park in partial fulfillment
of the requirements for the degree of
Master of Science
2012

Advisory Committee:

Professor José Luis Contreras-Vidal, Chair
Assistant Professor Dan Butts
Professor Shihab Shamma

Acknowledgements

I would like to thank my advisor, José "Pepe" L. Contreras-Vidal, first and foremost for his mentorship and support with this project; Larry Forrester and the staff at the Human Motor Performance Laboratory at the Baltimore VAMC for assisting with the data collection; Harshavardhan Agashe, Andrew Paek, and Alessandro Presacco for their contributions and advice; and the participants who volunteered their time for this study.

Part of this work was previously presented at the 40th annual Neural Interfaces Conference in Salt Lake City, Utah, June 18-20, 2012, and the Society for Neuroscience Annual Meeting in New Orleans, Louisiana, October 13-17, 2012.

This study was supported by NINDS R01NS075889 and University of Maryland Baltimore's Pepper Pilot Study Award.

Table of Contents

List of Tables

List of Figures

List of Abbreviations

BMI – Brain-Machine Interface

ECoG – Electrocorticography

EEG – Electroencephalography

ERD – Event-Related Desynchonization

fMRI – functional Magnetic Resonance Imaging

PSD – Power Spectral Density

1. Introduction

1.1. Stroke and Motor Control

Stroke is the single leading cause of neurological disability in the United States, accounting for nearly 800,000 new or recurrent cases each year [1-2]. The disruption of blood flow to the brain, whether by restriction (ischemia) or internal bleeding (hemorrhage), is not fatal in most cases, with approximately 550,000 survivors, but most still experience some loss of brain function and motor impairment [3-4]. Hemiparesis is the primary cause of post-stroke disability and asymmetrically affects walking, limiting mobility and increasing dependency on assistance for daily life. Motor disability due to stroke is a different type of problem than disability due to spinal cord injury or loss of a limb from amputation; in the stroke case, the musculoskeletal system is still mostly intact and residual movement may still be present, but the proper control signal from an undamaged central nervous system necessary for natural volitional movement is lacking.

Recovery of motor function often occurs naturally to some degree in the months following stroke, and the extent and speed of recovery can usually be accelerated through rehabilitative therapies [5-8]. Patients can engage in repetitive and controlled tasks with their affected limbs to increase strength and dexterity from whatever residual movement may be left. But even with such therapies, improvement usually plateaus within three-six months [7-8]. Thus, a more viable solution is needed for extended recovery or for patients to be able to control and use a prosthetic device to improve quality of daily life. One such

solution that is currently a major topic of neuroscience and biomedical research involves extracting signals from brain activity for control of a movement-assist device that would engage the affected limbs into the desired movement. Such prostheses may even be temporary solutions that serve to speed rehabilitative recovery until the patient has regained full strength and control.

1.2. Physiological Changes in the Brain after Stroke

Decoding motor intent from neural activity in stroke survivors presents a new problem compared to understanding motor intent in healthy subjects; there are significant physiological damages to the brain as well as brain reorganization as a result of stroke, and the extent to which relevant information can be extracted is unclear. Extensive work has indicated that motor cortex contralateral to limb movement encodes information of motor intent [8-11], with a separate and distinct physiology in the ipsilateral cortex possibly thought to be associated with motor planning [12]. Stroke-induced lesions often cause hemiparesis characterized by impaired contralateral motor execution. It is thought that the damage due to these lesions distorts the motor information available from the affected hemisphere and may no longer provide a usable control signal for a movement-assist device.

Imaging studies using functional magnetic resonance imaging (fMRI) have given insight into different activation patterns in the brain following stroke. Patients have been known to exhibit more bilateral activation in the motor cortex after early and chronic stroke, suggesting recruitment of neurons from cortex ipsilateral to movement. The intensity of

the activation from the unlesioned hemisphere (in primary sensorimotor and supplementary motor areas) was correlated with the severity of disability, and bilateralness was also shown to decrease with recovery as motor function improved [13-15]. Imaging in recovered patients show enlarged activation in primary and sensorimotor motor cortices in the lesioned hemisphere, and recruitment of sensorimotor areas on the contralesional side [16-19], characterizing the type of reorganization of neural circuitry from rehabilitative therapies. Locomotive training in particular has been shown to improve walking function and elicit plasticity in the central nervous system [7, 20]. Variability in the types of stroke and lesion locations also results in different activation patterns (subcortical stroke saw recruitment of standard motor circuitry, whereas cortical stroke involved alternative networks), suggesting lesion-specific mechanisms of reorganization [16].

Electrophysiological techniques such as electroencephalography (EEG) and electrocorticography (ECoG) have also been used to explore the lesional affects due to stroke. EEG studies have shown decreased event-related desynchronizations (ERDs), the decrease in power of a certain frequency range, in the 8-12 Hz alpha rhythms (also known as mu-band) in patients who have suffered cortical strokes during upper limb movements; there was an even smaller alpha ERD in the affected hemisphere versus the healthy hemisphere during respective contralateral hand movements. When attempting to control the paretic hand, contralesional alpha ERD was stronger than ipsilesional ERD; ipsilesional ERD amplitude was better preserved for non-paretic movement than with paretic movement [21-22]. A case study measuring ECoG in a stroke victim reported

changes in beta band (12-30 Hz) amplitude in different hand movements (both hands or paretic hand only) otherwise not seen in healthy subjects [23]; the beta band is associated with thalamic projections to the cortex [24] and the newly observed change suggests that the reorganization involves a thalamo-cortical mechanism common between the different movement types.

1.3. Previous Efforts in Decoding Movement from Neural Signals

The large majority of prior stroke-related work in neural decoding of movement has primarily been done with upper limb movements in arm reaching or hand grasping. Some of these studies analyzed only signals from the contralesional hemisphere, bypassing the areas affected by the stroke lesions. Attempts to decode intent to raise either the affected or unaffected arm saw similar successful decoding accuracy regardless of arm, suggesting that the contralesional hemisphere is sufficient for control of motor rehabilitation prosthetics [22]. Another study identified the distinctions in the signals from the contralesional hemisphere when moving either the ipsilateral (paretic) or contralateral hand, and to use the features associated with moving the affected hand for cursor control in a brain-machine interface (BMI) system (simulated hand movement) [8].

Two studies reported the use of whole-scalp EEG (including the areas affected by stroke) to detect intent to open and close the hand [5-6]. By continuing to use signals from the damaged areas, these studies speculate a more effective approach to rebuild the lost neural circuits through use-dependent plasticity. Synapses are strengthened through spike timing-dependent plasticity when pre-synaptic neurons fire action potentials immediately

before the post-synaptic neuron fires [25]. In the context of stroke rehabilitation, enforcing the movement of the paretic arm either by a movement-assist device or neuromuscular stimulation immediately after motor signals are detected in the ipsilesional hemisphere will maximize plasticity and lead to faster and fuller motor recovery.

Decoding of walking or other leg movements has yet to be attempted in stroke patients, and has only seen limited success in healthy subjects and animal studies. Surgically-implanted intracortical electrodes were used to record action potential spikes from the motor cortex in rhesus macaques during a bipedal walking task; the recorded firing rates were used to decode the kinematic parameters of the monkeys' hip, knee, and ankle joints offline and in real-time [26]. This was emulated in a similar study using EEG recorded from healthy human subjects, in which EEG amplitudes were used to decode the same kinematic parameters offline with comparable accuracy [27-28]. Additional work in decoding walking from EEG is limited due to the notion that despite the similarly successful results, EEG has insufficient spatial resolution and signal-to-noise ratio compared to invasive recording methods for BMI and neuroprosthetic applications [29].

1.4. Objectives

This study explores the hypothesis that walking can be decoded noninvasively from stroke survivors in the same manner as the previously discussed walking studies [26-28]. This hypothesis is based on the rationale that as previous attempts to decode upper limb movements in healthy subjects have been successfully translated to decoding the same

movements in stroke patients, it is likely that similar methods and techniques can be employed to translate the successes from walking studies likewise. This study aims to meet the following objectives:

1. Examine and compare the power spectral density of the EEG of stroke subjects and healthy controls during walking and at rest.
2. Evaluate and compare the performance of a Wiener Filter and an n^{th}-order Unscented Kalman Filter in decoding joint kinematics of stroke subjects during treadmill walking from their EEG.
3. Provided the previous objective is fulfilled, determine the neural cortical contributions to walking in stroke patients.

2. Methods

2.1. Subjects

Subjects for this study were recruited with the requirement that they must:

- be between 21 and 85 years of age
- have had an ischemic or hemorrhagic stroke more than 3 months prior
- be physically able to participate in the testing protocol
- have residual hemiparetic gait with observable asymmetry in the gait pattern
- have completed all conventional physical therapy
- have adequate language and neurocognitive function to participate in training, testing, and to give informed consent

Four adults, aged 50-64 (3 males, 1 female) and all left paretic, were enrolled in the study having met the above requirements and providing informed consent. Table 1 contains detailed information about each subject. Lesion locations were obtained from individual medical records and confirmed by radiologic reports of CT or MRI images. Some information is missing since they were not provided by the subjects' nurse practitioners or medical examiners. One additional healthy subject (male, 28) with no history of neurological disease or lower limb pathology and free of injury participated in the study as healthy control subjects after giving consent. The study was conducted with approved protocols from the Institutional Review Boards at University of Maryland College Park, University of Maryland Baltimore, and the Baltimore VA Research and Development Committee.

Table 1. Detailed Information for Study Participants

Subject	S1	S2	S3	S4
Gender	M	M	F	M
Age	56	50	64	60
Time Since Stroke	9m, 12d	8y, 7m, 11d	9y, 7m	1y, 9m, 19d
Paretic Leg Strength (Manual Muscle Test)	N/A	4	2	N/A
Self-Selected Walking Speed (km/h)	1.8	2.2	0.3	1.5
CVA Type	Hemorrhagic	Ischemic	Ischemic turned into hemorrhagic	Ischemic
Paretic Side	L	L	L	L
Lesion Location	R basal ganglia	Bilateral lesions: bilateral cerebellum R thalamus, L occipital	R middle cerebral artery (ischemic), R basal ganglia (hemorrhagic)	R middle cerebral artery with lesions in R temporal lobe insular cortex and R basal ganglia

2.2. Experimental Setup and Procedure

Participants were first asked to establish their most comfortable walking speed (self-determined) while walking on a treadmill during a two-minute familiarization period that preceded the recording trials. A two-minute baseline EEG was recorded while the participant remained standing, at rest.

For the main experimental task, the participants were asked to perform five minutes of "precision walking". Participants would walk on the treadmill at their pre-selected comfort pace and watch a video monitor directly in front of them providing real-time visual feedback of the position of their feet via a digital video recorder recording at 30 frames/s. A white stripe (2 inches wide) was drawn diagonally along the treadmill belt at approximately a 45^{o} angle from the edge. Participants were asked to avoid stepping on

this line using the visual feedback from the monitor. This paradigm increases the attentional demands of the walking task and simulates walking in a novel environment and/or under novel conditions [30].

An additional session of recording was done while the participant was at rest, sitting, and watching the video playback of their feet walking during the precision task, evoking responses to motor imagery.

Figure 1 shows a photograph of one of the control subjects in the experimental setups, fitted with motion sensors and EEG cap.

Figure 1. Control subject in the experimental setup, fitted with motion sensors and EEG cap [27]

2.3. Motion Capture and EEG Recording

Three-dimensional joint kinematics of the left and right hip, knee, and ankle joints were recorded using an infrared motion capture system (Optotrak, Northern Digital, Ontario, Canada) at 100 Hz. Precision manufactured 5 cm discs (Innovative Sports Training, Chicago, IL), each embedded with three infrared diodes, were fixed with adhesive and secured with foam wrap at the participants' second sacral vertebra (S2) and in the middle of the thighs, shanks, and foot segments of both legs. Motion analysis software (Motion Monitor, Innovative Sports Training, Chicago, IL) created a segmental model of the legs by digitizing the joint centers for the hip, knee, and ankle joints, and derived the gait kinematics, exporting the time histories of the *x*, *y*, and *z* positions, joint angular position, and joint angular velocity for the six joints.

Whole scalp 64-channel EEG data were collected (actiCap system, Brain Products GmbH, Munich, Germany) and labeled in accordance with an extended 10-20 international system [31] (Figure 2). The EEG data were online referenced to the right earlobe with a common ground at the FPz site. Electrode impedances were maintained below 10 kΩ with bandpass filters set at 0.01-100 Hz with a sampling rate of 1 kHz. The EEG signal was digitized using a BrainAmp DC amplifier linked to BrainVision Recorder software version 1.10. The EEG data were time-locked with the movement kinematics data using footswitch signals added into the datasets (Koningsberg Instrumentation, Pasadena, CA).

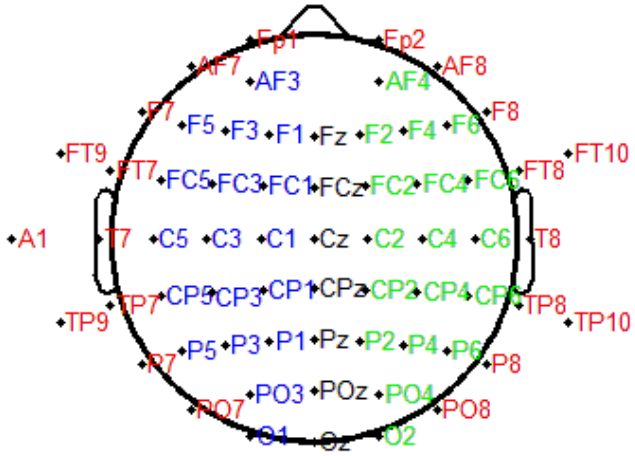

Figure 2. EEG Channel Locations (Red denotes periphery electrodes removed from analysis, Blue denotes left hemisphere channels, and Green denotes right hemisphere channels)

2.4. Power Spectral Density Analysis

The power spectral density (PSD) describes how the power of a signal is distributed as a function of frequency, and is computed as the discrete-time Fourier transform of its auto-correlation. The PSD for the EEG data for the stroke subjects and healthy controls during walking and rest were computed using Thomson's adaptive multitaper method [32-33], with a time-bandwidth product of 4 and a frequency resolution of 0.1 Hz.

The PSD was calculated from minute-long segments of the EEG data for each channel. The average PSD was computed by averaging across all segments for each subject at rest and during the precision walking task, and for bilateral, left hemisphere, and right hemisphere conditions of electrode selection (see *Signal Preprocessing)*. All PSD averages were smoothed with a moving average filter with a span of 11.

All data processing was done offline in Matlab (Mathworks Inc., Natick, MA).

2.5. Signal Preprocessing

The EEG data were first re-referenced offline to both mastoids. The EEG values from the channel at the centroid position of the scalp (CZ) were subtracted from all other channels; the mean of the mastoid channels was computed by averaging the data from channels A1 and A2 (initially at zero, but now corresponding to the negative of the original CZ), and this mean was subtracted from all other channels. All periphery channels were removed for offline analysis: the most frontal channels (Fp1, Fp2, AF7, AF8, F7, F8), all of the temporal channels (all channels labeled FT, T, TP, and P7, PO7, P8, PO8), and the left earlobe (A1); these channels are most susceptible to artifacts from eye-blinks and facial/cranial muscle activity [34]. The remaining channels were assigned to the left hemisphere if given an odd numbered label, and to the right hemisphere if given an even numbered label (Figure 2). Hemispheric analyses were done by repeating the processing and decoding steps excluding the right and left channels in turn.

Both kinematic and EEG data were segmented into five minute-long segments for cross-validation purposes (see Model Performance Metrics). The EEG signals were downsampled by a factor of 10 (from 1000Hz to 100Hz, to match the sampling rate of the kinematics); processed with a zero-phase, fourth order, band-pass Butterworth filter (0.1–3 Hz), isolating the delta band of EEG; and normalized by subtracting their mean and dividing by their standard deviation. The kinematic data were processed with the same filter, given that this frequency range has been shown to contain 90% of the original power in walking [27]. Slower gait speeds in stroke hemiplegics would likely concentrate the frequency content in lower regions, making 3 Hz a more conservative cutoff.

The EEG data were compiled into a large feature matrix, with each row representing data from a single sample of time, and containing the EEG voltages at all remaining channels and the voltages at different time lags for each channel. Principal component analysis (PCA) was applied to this data matrix to reduce the high dimensionality (number of channels times number of time lags). PCA projects the data matrix onto a smaller subset of eigenvectors that account for 99% of the variance in the data; in this analysis, dimensionality was reduced by an approximate factor of 10, greatly reducing computational complexity and reducing overfitting. Kinematic data were separated by joint and compiled in similar data matrices, with each row containing the values of the different kinematic parameters at each time sample.

The processing steps are summarized in the flowchart in Figure 3.

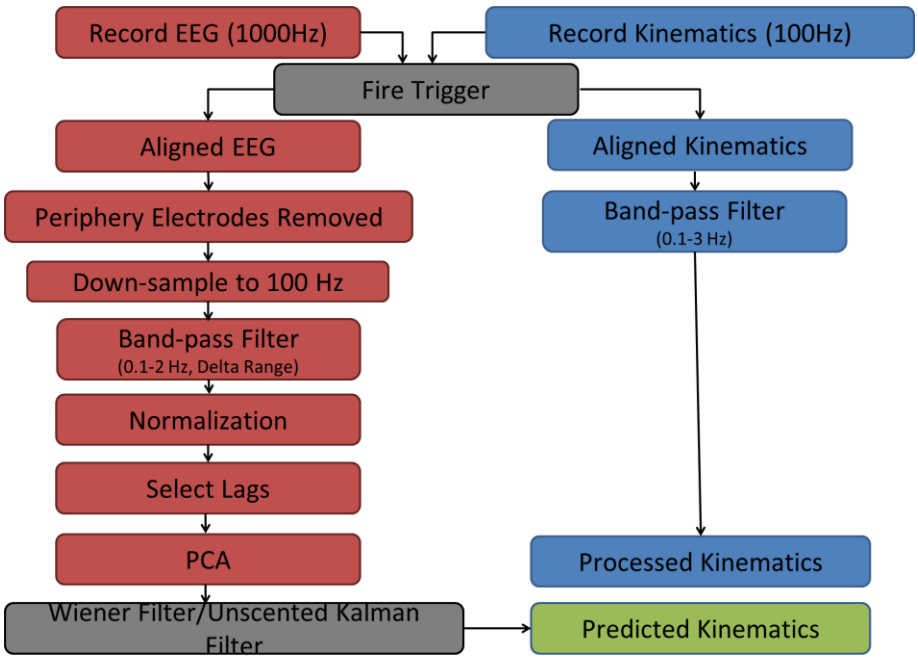

Figure 3. Flowchart of processing steps for EEG and kinematic data

2.6. Decoding Algorithms

Two different decoding algorithms were used to predict the kinematic variables of the joints from the EEG signals: the Wiener Filter and the nth order Unscented Kalman Filter.

The model for the Wiener filter was given by the linear equation:

$$x(t) = b + \sum_{i=1}^{N}\sum_{j=1}^{L} w_{ij} n_i\left(t - l_j\right) + \varepsilon(t)$$

in which $x(t)$ is the time series of the gait parameter measured (*x, y, z, φ, dφ/dt*) representing the Cartesian positions and angular position and velocity for the left and right hip, knee, and ankle joints; *L* and *N* are the number of lags and electrodes respectively; $n_i\left(t - l_j\right)$ is the standardized EEG voltage measured at electrode *i* at time lag l_j, where l is the nonlinear vector of time lags {0, 1, 2, 3, 4, 5, 6, 7, 8, 9, 10, 15, 20, 25, 30, 40, 50, 60, 80, 100} in units of samples 10 ms apart; *b* and w_{ij} are weights obtained through solving the least squares equation; and $\varepsilon(t)$ is the residual error. The equation expresses the kinematics as a weighted sum of the EEG voltage amplitudes at present time and at previous time steps. The nonlinear time lag vector allows contributions going as far back as 1 second into the past, spanning periods of motor planning. The Wiener Filter equation can be expressed in matrix form as

$$\boldsymbol{X} = \boldsymbol{NW} + \varepsilon,$$

where $\boldsymbol{X}$ is the matrix of all kinematic parameters for each joint, $\boldsymbol{N}$ is the matrix of EEG amplitudes, and $\boldsymbol{W}$ is the matrix of weights, and ε is the error vector. Then the least squares solution to solve for the weight matrix is given by [26-28, 35]:

$$W = inv(N^T N)N^T X.$$

The n^{th} order Unscented Kalman Filter is an extension of the Kalman Filter state space algorithm, which recursively makes estimates of kinematics and error covariance from the previous time step, and combines these estimates with EEG data to make predictions. The Kalman filter does not have the same stationary assumptions that the Wiener filter has, and its recursive property makes it more ideal for real-time applications. An n^{th} order filter makes kinematic predictions from the previous n-1 time steps. The unscented transform represents the distribution of the kinematics by a Gaussian random variable by a careful selection of sample points that capture the true mean and covariance of the kinematics, which can also be propagated through nonlinear neural tuning models. The neural tuning model actually makes an estimate of the EEG voltages from the past predicted kinematics, and uses the error in the estimate to adjust the gain that propagates the current kinematic prediction to the next prediction [36-37]. The nonlinear tuning model expressed the EEG voltages *y(t)* as a function of the kinematic parameters:

$$y(t) = b_1\phi(t) + b_2\frac{d\phi(t)}{dt} + b_3 pos_x(t) + b_4 pos_y(t) + b_5 pos_z(t) + b_6\sqrt{pos_x(t)^2 + pos_y(t)^2 + pos_z(t)^2}$$

since it has been shown that this function was optimized for neural spike tuning in a reaching decoding study [37]. Table 2 contains the equations for the Kalman Filter and the Unscented Kalman Filter.

Table 2. Comparison of equations for the standard Kalman filter and the unscented Kalman filter [37]

	Kalman filter	Unscented Kalman filter
Predict step	$\mathbf{x}_{t'} = \mathbf{F}\mathbf{x}_{t-1}$	$\mathbf{x}_{t'} = \mathbf{F}\mathbf{x}_{t-1}$
	$\mathbf{P}_{t'} = \mathbf{F}\mathbf{P}_{t-1}\mathbf{F}^T + \mathbf{Q}$	$\mathbf{P}_{t'} = \mathbf{F}\mathbf{P}_{t-1}\mathbf{F}^T + \mathbf{Q}$
Update step		$X_0 = \mathbf{x}_{t'}$
		$X_i = \mathbf{x}_{t'} + \left(\sqrt{(d+\kappa)\mathbf{P}_{t'}}\right)_i \quad i = 1 \dots d$
		$X_i = \mathbf{x}_{t'} - \left(\sqrt{(d+\kappa)\mathbf{P}_{t'}}\right)_{i-d} \quad i = d+1 \dots 2d$
		$w_0 = \frac{\kappa}{d+\kappa} \quad w_i = \frac{1}{2(d+\kappa)} \quad i = 1 \dots 2d$
		$Z_i = h(X_i) \quad i = 0 \dots 2d$
	$\mathbf{z}_t = \mathbf{H}\mathbf{x}_{t'}$	$\mathbf{z}_t = \sum_{i=0\dots2d} w_i Z_i$
		$\mathbf{P}_{zz,t} = w_0(Z_0 - \mathbf{z}_t)(Z_0 - \mathbf{z}_t)^T + \left(\sum_{i=1\dots2d} w_i(Z_i - Z_0)(Z_i - Z_0)^T\right) + \mathbf{R}$
	$\mathbf{S}_t = \mathbf{H}\mathbf{P}_{t'}\mathbf{H}^T + \mathbf{R}$	$\mathbf{P}_{xz,t} = w_0(X_0 - \mathbf{x}_{t'})(Z_0 - \mathbf{z}_t)^T + \left(\sum_{i=1\dots2d} w_i(X_i - X_0)(Z_i - Z_0)^T\right)$
	$\mathbf{K}_t = \mathbf{P}_{t'}\mathbf{H}^T\mathbf{S}_t^{-1}$	$\mathbf{K} = \mathbf{P}_{xz,t}\mathbf{P}_{zz,t}^{-1}$
	$\mathbf{x}_t = \mathbf{x}_{t'} + \mathbf{K}_t(\mathbf{y}_t - \mathbf{z}_t)$	$\mathbf{x}_t = \mathbf{x}_{t'} + \mathbf{K}_t(\mathbf{y}_t - \mathbf{z}_t)$
	$\mathbf{P}_t = (\mathbf{I} - \mathbf{K}_t\mathbf{H})\mathbf{P}_{t'}$	$\mathbf{P}_t = \mathbf{P}_{t'} - \mathbf{P}_{xz,t}\left(\mathbf{P}_{zz,t}^{-1}\right)^T\mathbf{P}_{xz,t}^T$

2.7. Model Performance and Metrics

A five-fold cross-validation procedure was used to assess the generalized performance of the decoders on independent data sets. The five-minute precision walking session was divided into five one-minute fold segments. Four folds would be used to train the decoders (decoders were trained independently for each subject and for each joint), and the decoding parameters would be applied to the last fold as a test set. The procedure was repeated five times to ensure that each fold was used as the test set, and the performances were averaged across folds.

Prediction accuracy of the decoders was measured by Pearson's correlation coefficient, *r*, between the measured kinematic signal and the predicted output, given by the equation:

$$r(x, \hat{x}) = \frac{cov(x,\hat{x})}{\sigma_x \sigma_{\hat{x}}},$$

where x is the measured kinematic signal, $\hat{x}$ is the predicted signal, and σ_x and $\sigma_{\hat{x}}$ are the respective standard deviations of x and $\hat{x}$. The values of *r* range from -1 to 1, with 1 indicating the strongest correlation, i.e. perfect prediction, 0 implying no correlation, and -1 implying that the prediction and actual signals are anti-correlated [26-28].

2.8. Scalp Map and Lag Selection Analysis

The Pearson's correlation coefficient expresses performance only as a function of all variables used in the decoder without indicating their individual contributions. The data used in the decoder itself does not reflect actual EEG data, but only the principal components derived from eigenvector projections in PCA. The weight matrix $\boldsymbol{W}$ in the Wiener filter contains coefficients for the reduced number of features in the principal components. The weights were mapped back to the full dimension space by reverse projecting the PCA coefficient matrix onto $\boldsymbol{W}$, giving us the coefficients of the linear decoder in terms of EEG electrode channels and time lags.

To analyze the contributions of electrodes only, the rows of the new coefficient matrix corresponding to different time lags for the same sensor were averaged, yielding a vector for each joint's kinematic parameter, with entries corresponding to the electrode channels. The vectors for the kinematic parameters of joints on the same leg were averaged together. The *topoplot* function of EEGLAB [38] mapped these coefficients onto a scalp map. Similarly, the contributions of the individual lags were analyzed by averaging the rows corresponding to the same lag but different electrodes. This analysis was done for each stroke subject and for the healthy controls.

3. Results

3.1. Spectral Signature of EEG during Walking

The power spectral density computed for the EEG of all subjects during the walking task is shown in Figure 4. The PSD function describes the amount of energy distributed at each frequency in the signal. Our healthy control (H1) shares the same spectral signature as was found in a prior study involving precision walking [27], and the PSD functions for the stroke subjects follow the same general shape. Variability in the stroke lesions is expected to have different effects on the overall physiological characteristics of the brain to some degree, and as such there is some variability in the spectral signature for different stroke patients: subjects S2 and S3 have significantly more power between 2 and 9 Hz (overlapping the delta and theta bands). Power beyond the alpha band (i.e. > 13 Hz) tends to converge for all subjects, although the power in S1 drops drastically after 10 Hz. One common characteristic among the PSD plots for the stroke subjects is the shift in the hump found in the alpha/mu band (8–13 Hz) of the healthy control. This hump appears at lower frequencies (closer to the 5-10Hz range) for all stroke subjects.

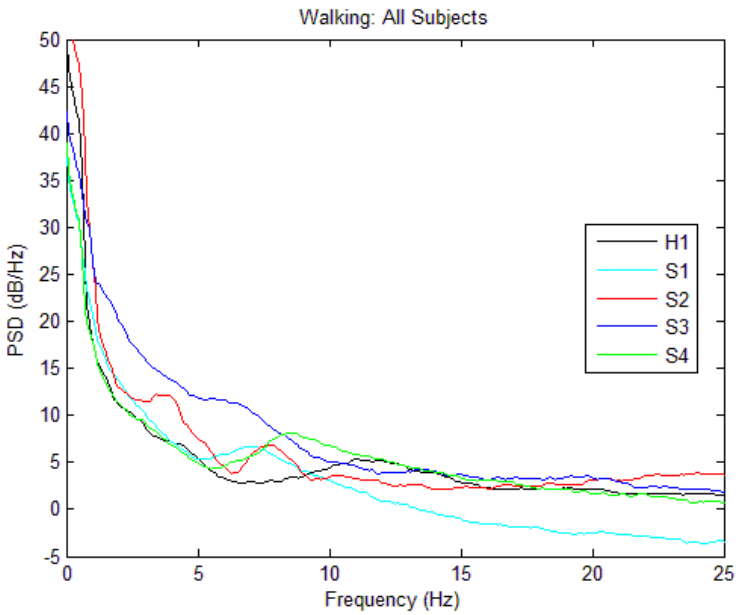

Figure 4. Power spectral density for all subjects during precision walking task

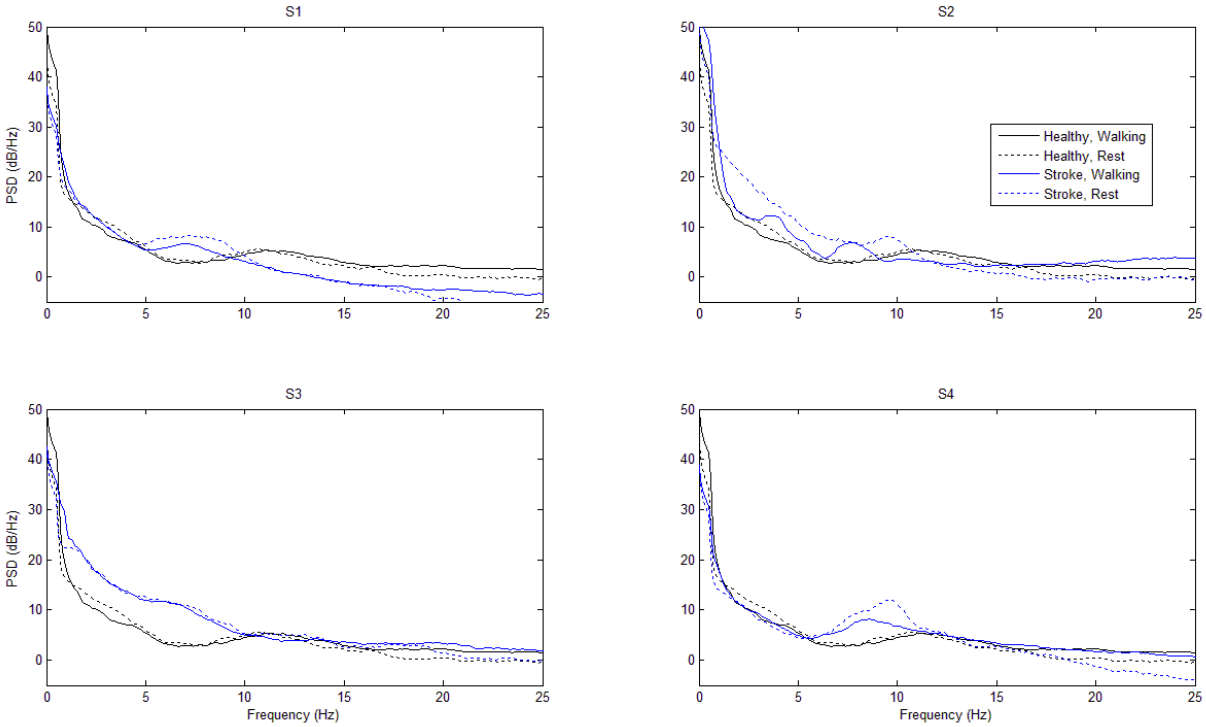

Figure 5. Power spectral density: walking vs. rest

The PSD during walking is compared with the PSD during rest in Figure 5. Previous literature suggests suppression in the mu band (8–13 Hz) during movement [27, 39], and decreased event-related de-synchronization (ERD) for movement in the same range after a stroke [21]. As mentioned before, the "mu band hump" in the healthy PSD had shifted downwards in the stroke PSD; it can be seen that the resting PSD is indeed greater in this frequency range for S1, S2, and S4. The amount of suppression does not seem to be reduced for stroke as was expected in [21]. Beyond this frequency range, power in the resting PSD is lower than during walking for all subjects. Another consistent finding with previous literature is that the PSD does not seem to be affected by walking in the low delta range (< 2 Hz) [27, 40].

The PSD was also analyzed by hemisphere, as shown in Figure 6. Left hemisphere (LH) and right hemisphere (RH) conditions were formed by removing all of the even-numbered electrodes in the right hemisphere or the odd-numbered electrodes in the left respectively (Figure 2). All stroke subjects were left paretic and had some amount of lesion in the right hemisphere; S2 had some amount of bilateral lesion. The differences between the PSD for different hemispheric conditions (each hemisphere individually and both together) were not significant. Previous literature [21] suggests that contralesional hemispheres would see more alpha/mu-ERD than ipsilesional hemispheres for paretic movements, but the two would be on par for non-paretic movement. Subjects show that the PSD of the ipsilesional (right) hemisphere during the shifted "mu band hump" is minimally, albeit insignificantly, greater than that of the contralesional (left), possibly

indicating less suppression from rest. But because bilateral walking involves paretic and non-paretic movements, that effect should not necessarily be strongly apparent.

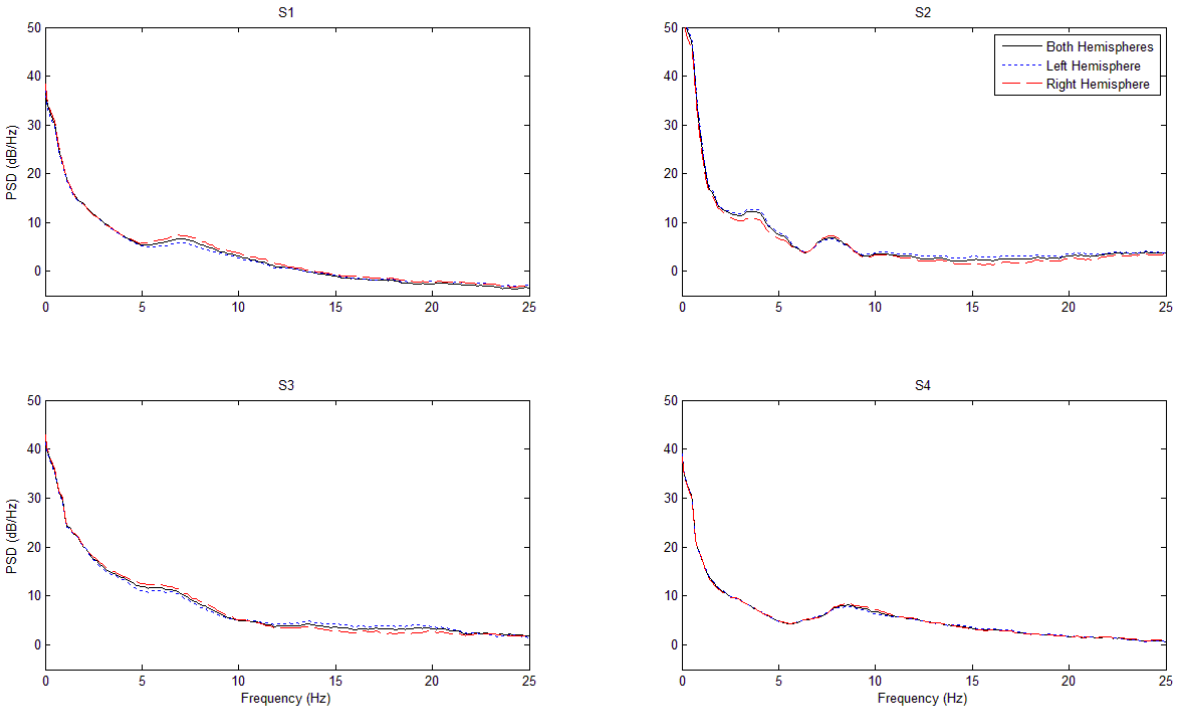

Figure 6. Power spectral density by hemisphere

3.2. Decoding Accuracies

Our decoders performed reasonably well in being able to predict and reconstruct the Cartesian position, angular position, and angular velocity of the hips, knees, and ankles from EEG during the precision walking task. Reported *r* values corresponding to the Pearson's correlation coefficient were not as high as has been reported in decoding from healthy subjects or from implanted electrodes in monkeys [26-27], but with an overall *r* value of 0.52 ± 0.2, indicating moderate correlation between the decoded prediction and the true signal.

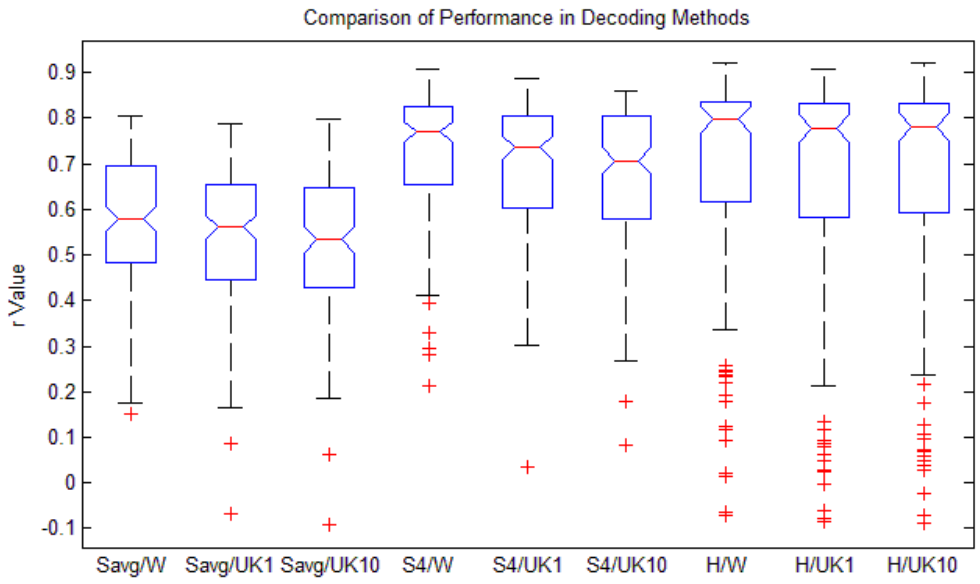

Figure 7. Box plots showing the distribution of *r*-values for the different decoding methods (Subject/Decoder)

The box plots in Figure 7 show the statistics for the *r* values for the different decoders used averaged across all stroke subjects (Savg), for the best decoded subject (S4), and for the healthy control (H). Boxes whose notches do not overlap indicate that their true medians differ from each other with 95% confidence. General trends show decreasing medians between the three methods although not necessarily within the 95% confidence interval. The Wiener filter (W) generally yielded higher *r*-values than the unscented Kalman filter (UK), whose decoding accuracies had an overall better distribution than the 10^{th} order unscented Kalman filter (UK10). While the average stroke decoding was significantly worse than the healthy control (but with median $r > 0.5$, moderate correlation), the best decoded stroke subject was about on par with the control for the Wiener and first order unscented Kalman, but not the 10^{th} order.

The ability of the Wiener filter to decode the kinematics of the individual leg joints averaged across all subjects is shown in the box plots of Figure 8. All subjects had an asymmetric gait, impaired by left hemiplegia. This did not affect the decoders' ability to reconstruct the kinematics for the affected joints: the left hip (LH), the left knee (LK), and the left ankle (LA). The decoding accuracies were about on par with the accuracies from the right joints: right hip (RH), right knee (RK), and right ankle (RA). A downward trend in the distribution of the *r*-values could be seen going from the hip to the knee to the ankle, although significance is only present between the hip decoding and the ankle decoding.

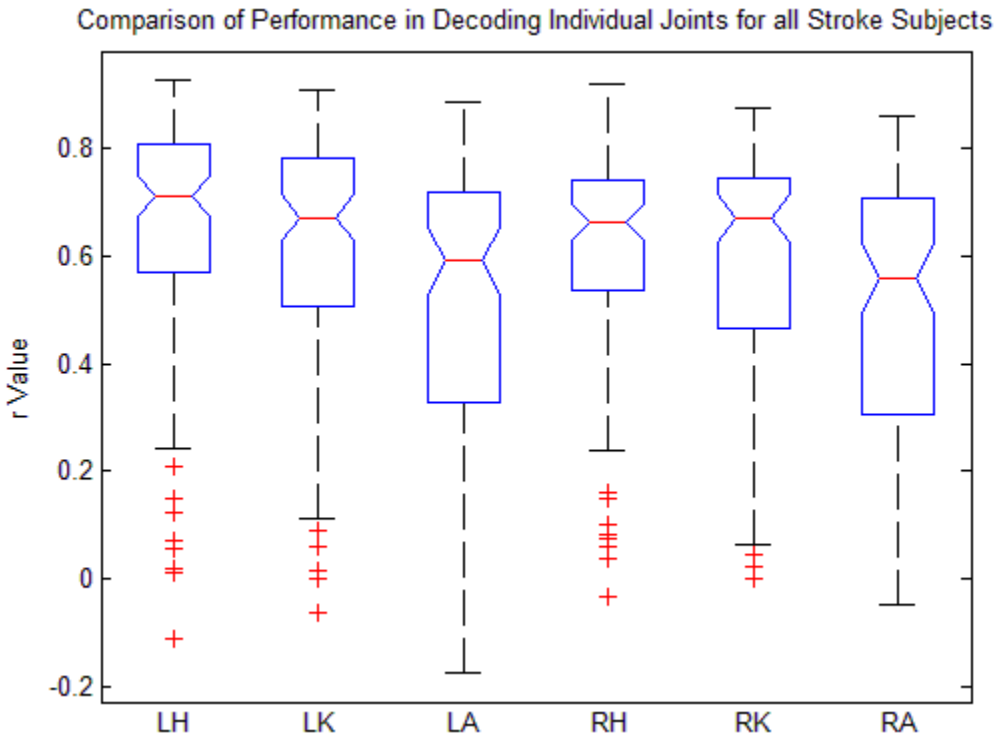

Figure 8. Box plots showing the distribution of *r*-values for the individual leg joints

Figure 9 and Figure 10 show the box plots for the *r*-values from decoding all joints and kinematic parameters on each individual leg from the different hemisphere conditions:

electrodes from left hemisphere only (L), electrodes from both hemispheres (B), and right hemisphere only (R). Figure 9 shows the distributions averaged across all subjects, and Figure 10 shows the distributions for each of the four stroke subjects. From Figure 9, there seems to be no significant difference in decoding either the paretic (left) or non-paretic leg, or from using any single hemisphere; utilizing bilateral electrodes does improve decoding despite the presence of the stroke lesion.

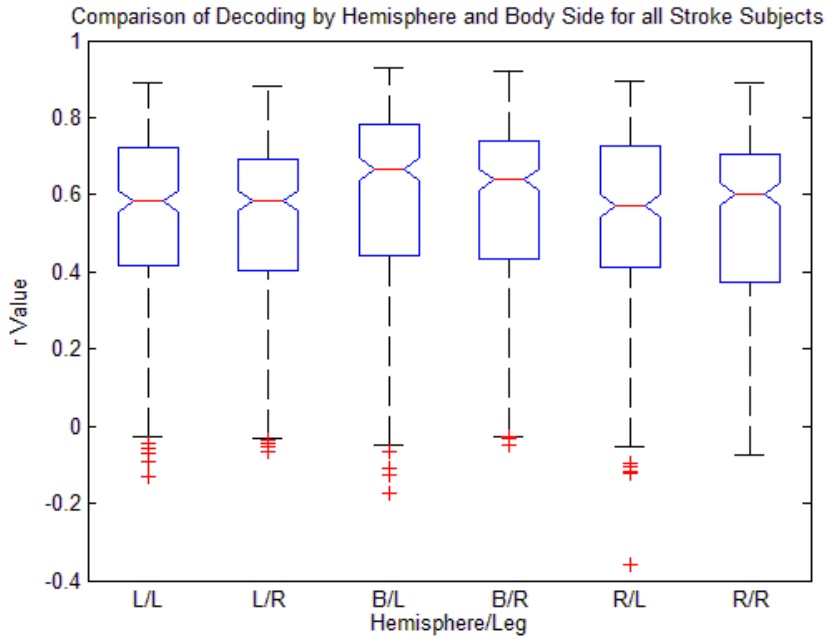

Figure 9. Box plots showing the distribution of *r*-values for different hemispheric conditions for all subjects

More variability when each subject is considered separately as in Figure 10. Subject S1 is the only subject that shows no change across all conditions, and also has the lowest median *r*-values (~0.33). All other subjects show higher decoding for the left paretic leg for all conditions (except for S2 when analyzing only the right hemisphere). But even here, decoding from the right hemisphere only versus the left hemisphere only did not

result in significantly different results; decoding from both together still yielded higher *r*–values than any of the two alone (significance in S2 and S3).

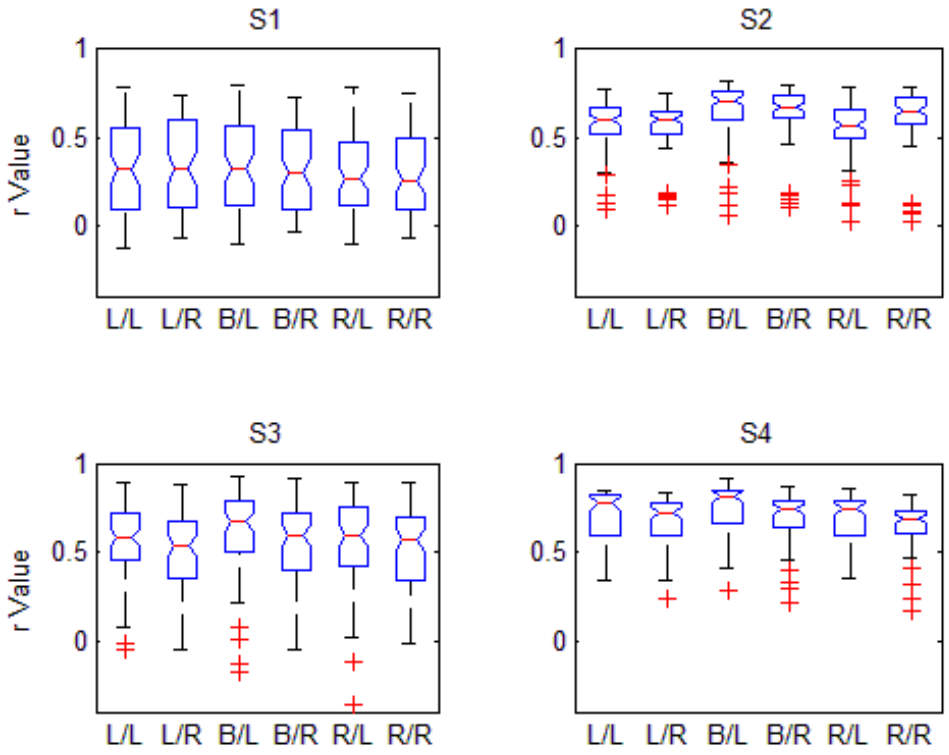

Figure 10. Box plots showing the distribution of *r*-values for hemispheric conditions for individual subjects (hemisphere condition / leg)

A better sense of decoding performance can be gleamed in Figures 11-13, which show the time course of the reconstructed and measured kinematics for the knees from S4 and for the left knee of the healthy control. The best-decoded fold is shown for the kinematic parameters from all decoding methods. Qualitative inspection indicates very reasonable reconstruction for nearly all parameters, with errors occurring most often in the x-coordinate and the angular velocity (for S4 only). In these examples, all of the decoding algorithms performed equally well. Qualitative differences can be seen in the kinematics of the paretic knee compared with the non-paretic knee and the healthy control.

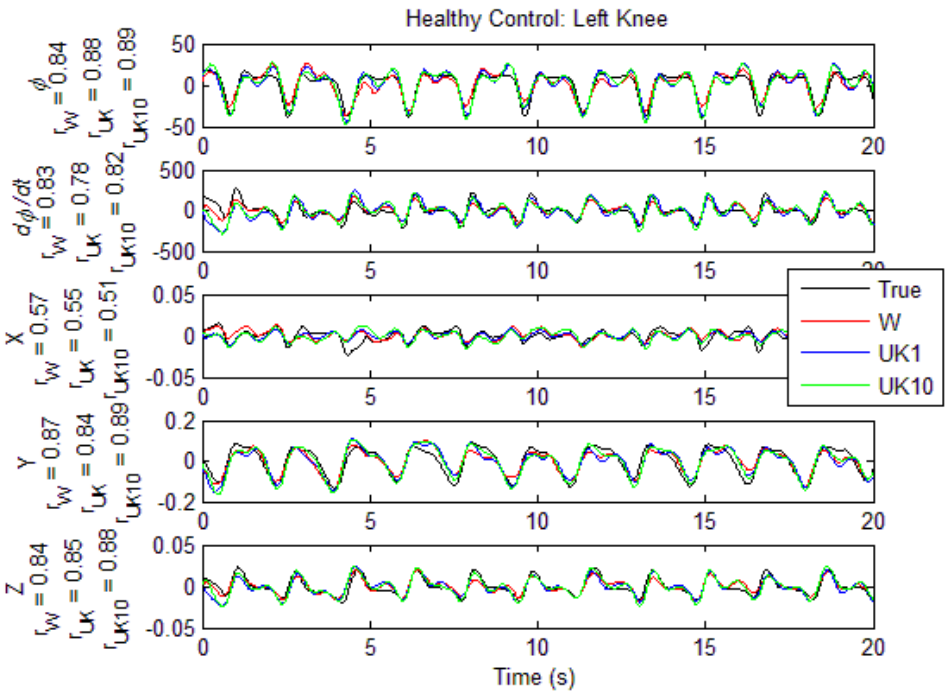

Figure 11. Measured and reconstructed time-courses for the kinematics for the left knee of H1

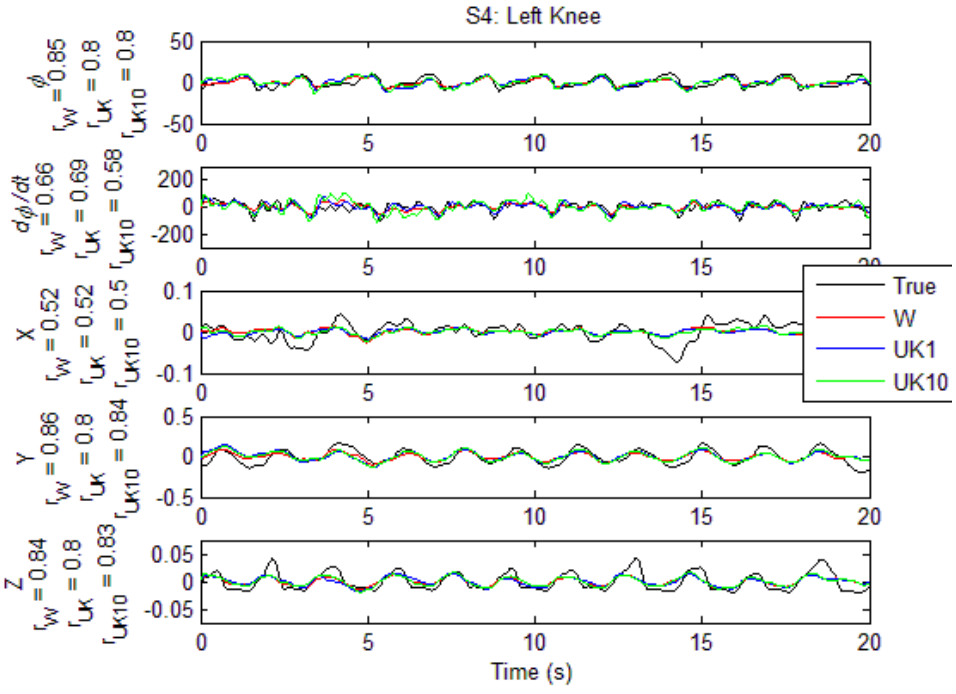

Figure 12. Measured and reconstructed time-courses for the kinematics for the left knee of S4

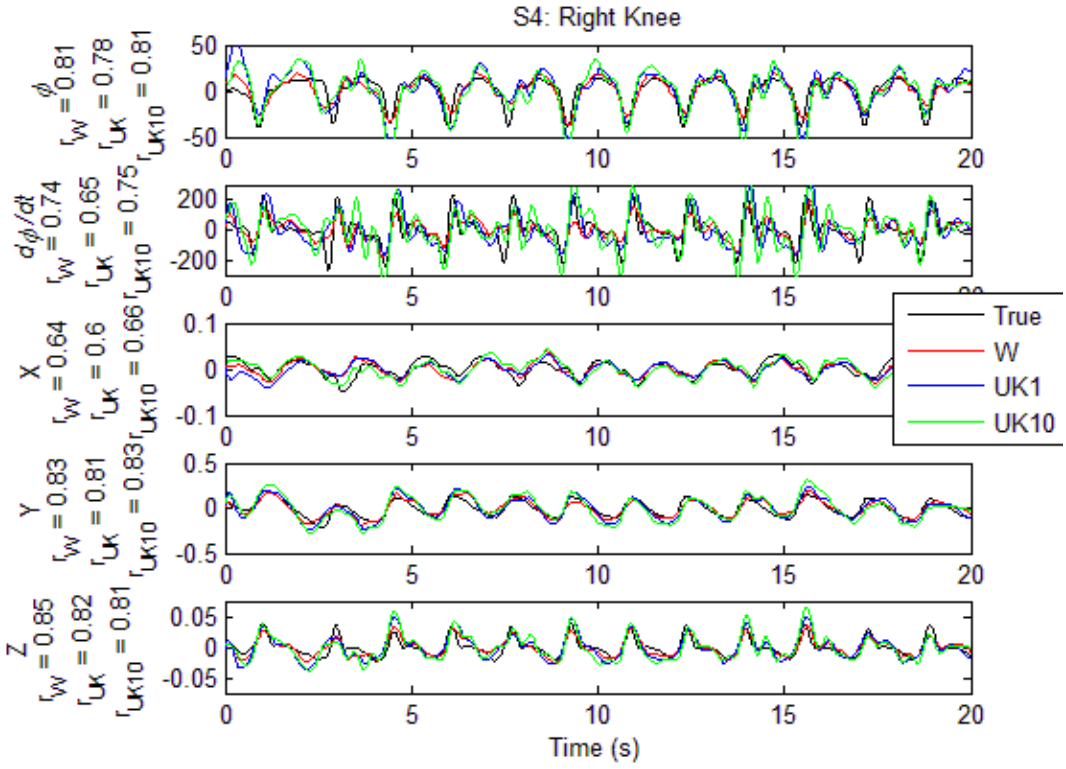

Figure 13. Measured and reconstructed time-courses for the kinematics for the right knee of S4

The means and standard deviations of all *r*-values are included in Table 3 for all subjects (S1, S2, S3, S4, H1, and the average of the stroke subjects), for all filters (Wiener, unscented Kalman, and 10th order unscented Kalman), for the different hemispheric conditions (left only, both, and right only), and for the joints and kinematic parameters of the left and right legs. Hemispheric analysis was not done for the healthy control.

Table 3. Mean and standard deviation of r-values for all subjects for all conditions and for all decoders

Electrodes Used	Leg	Decoder	S1	S2	S3	S4	S_{avg}	H1
Left Hemi-sphere	L	Wiener	0.320 ±0.26	0.569 ±0.14	0.550 ±0.21	0.704 ±0.15	0.536 ±0.24	
		Unscented Kalman	0.299 ±0.26	0.530 ±0.18	0.498 ±0.25	0.682 ±0.16	0.502 ±0.26	
		10^{th} Order UK	0.300 ±0.26	0.513 ±0.17	0.488 ±0.27	0.648 ±0.19	0.487 ±0.26	
	R	Wiener	0.352 ±0.26	0.572 ±0.13	0.500 ±0.22	0.670 ±0.14	0.523 ±0.23	
		Unscented Kalman	0.346 ±0.24	0.556 ±0.13	0.439 ±0.25	0.629 ±0.17	0.492 ±0.23	
		10^{th} Order UK	0.328 ±0.25	0.552 ±0.15	0.445 ±0.25	0.607 ±0.15	0.483 ±0.23	
Both Hemi-Spheres	L	Wiener	0.336 ±0.26	0.649 ±0.16	0.604 ±0.24	0.740 ±0.15	0.582 ±0.26	0.685 ±0.24
		Unscented Kalman	0.325 ±0.27	0.608 ±0.21	0.544 ±0.27	0.718 ±0.15	0.549 ±0.27	0.662 ±0.25
		10^{th} Order UK	0.311 ±0.26	0.581 ±0.20	0.533 ±0.29	0.696 ±0.16	0.530 ±0.27	0.669 ±0.26
	R	Wiener	0.331 ±0.24	0.645 ±0.15	0.557 ±0.22	0.699 ±0.13	0.558 ±0.24	0.699 ±0.22
		Unscented Kalman	0.327 ±0.23	0.635 ±0.15	0.475 ±0.26	0.660 ±0.15	0.524 ±0.24	0.655 ±0.26
		10^{th} Order UK	0.320 ±0.23	0.614 ±0.17	0.490 ±0.25	0.640 ±0.15	0.516 ±0.24	0.658 ±0.24
Right Hemi-Spheres	L	Wiener	0.295 ±0.23	0.555 ±0.15	0.554 ±0.26	0.692 ±0.13	0.524 ±0.25	
		Unscented Kalman	0.290 ±0.23	0.538 ±0.20	0.498 ±0.27	0.664 ±0.14	0.497 ±0.25	
		10^{th} Order UK	0.281 ±0.23	0.501 ±0.19	0.500 ±0.29	0.637 ±0.15	0.480 ±0.25	
	R	Wiener	0.298 ±0.23	0.616 ±0.17	0.531 ±0.22	0.649 ±0.12	0.523 ±0.23	
		Unscented Kalman	0.297 ±0.21	0.601 ±0.16	0.447 ±0.26	0.612 ±0.15	0.489 ±0.24	
		10^{th} Order UK	0.290 ±0.21	0.588 ±0.17	0.469 ±0.25	0.596 ±0.14	0.486 ±0.23	

3.3. Channel and Lag Weights

In order to identify the unique contributions the EEG channels and the time lags each had on the linear decoder model (Wiener filter), the coefficients matrix was projected back

onto spaces representing the individual channels and their time lags. The decoder did not process these directly, but instead processed the data transformed by PCA, so the coefficients were weights of the features of the principal components. The same PCA transform matrix was left-multiplied to the coefficient matrix to obtain a representation of the weights in terms of the channels and time lags. The weight contributions for a specific channel were found by summing all of the weights for that channel at the different time lags. These weights were projected onto scalp maps in Figure 14 for each subject and for the left and right joints separately.

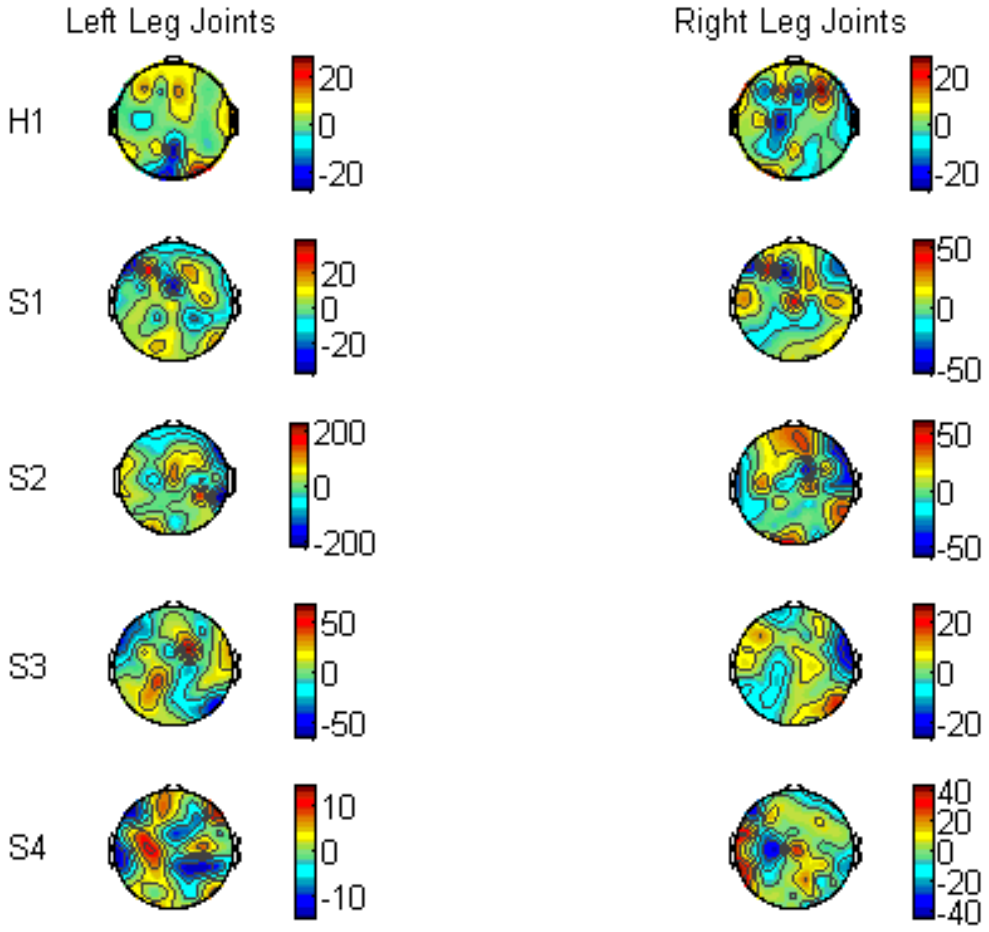

Figure 14. Scalp maps of the projected decoder weights for each electrode channel; color bar represents abstract units of coefficients mapping normalized EEG voltages to kinematic parameters

The distributions of the channel weights seem to vary considerably across subjects. The weights for the healthy control were most positive in frontal and right-most regions when decoding for left leg parameters, with strong negative weights posterior and in a small region on the left; the weights are more strongly negative for the right leg in the central regions and along the right of the scalp. All stroke subjects had lesions in the right hemisphere (S2 had bilateral lesions), although this did not seem to affect decoding performance as shown in Figures 9 and 10. Regions of negative weights do seem to be present in the right hemisphere for all stroke subjects when decoding parameters for the left leg, possibly trying to suppress whatever activity is due to lesioned areas; there was no negative region in the right hemisphere for the control.

Similarly the weight contributions for a specific lag were found by summing all of the weights for that lag across the different channels. These weights were plotted against their respective lags for all subjects in Figure 15. The values for the nonlinear time lag vector were: {0, 1, 2, 3, 4, 5, 6, 7, 8, 9, 10, 15, 20, 25, 30, 40, 50, 60, 80, 100} in units of samples 10 ms apart. The strongest weights, positive or negative, were usually located further away from 0. There also seems to be a sinusoidal pattern for the weights in a few of the subjects, and are slightly out of phase between the left and right leg.

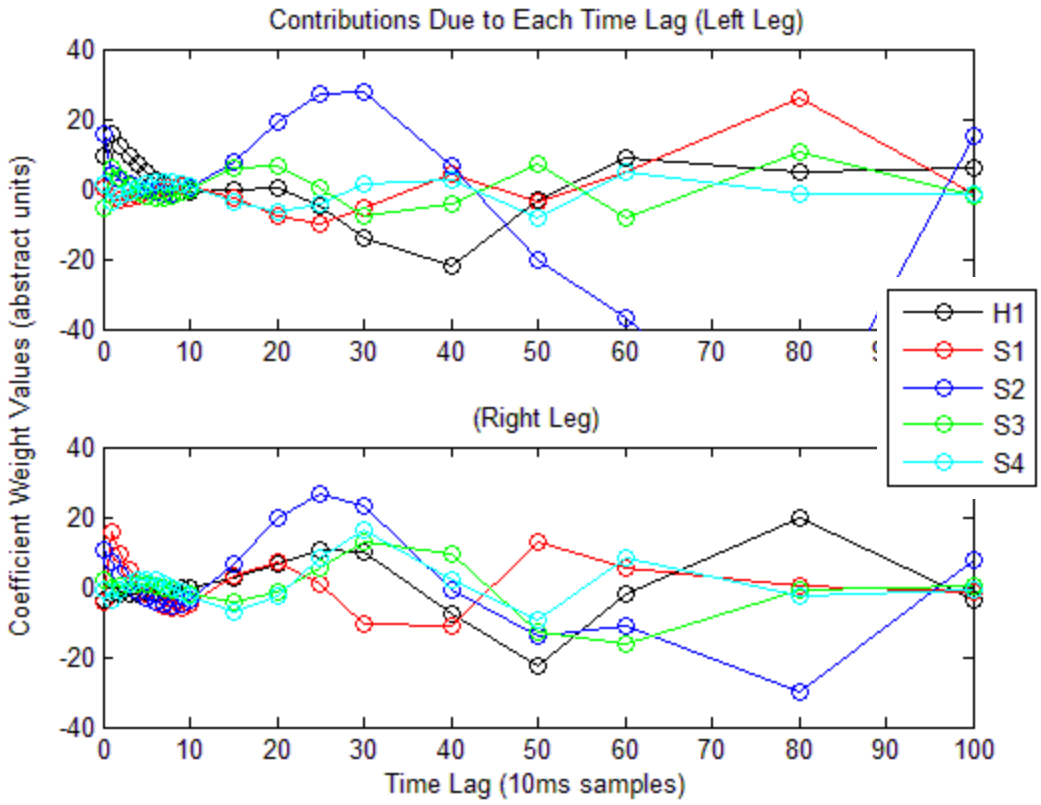

Figure 15. Plots of the projected decoder weights for each time lag for the left and right leg separately (y-axis represents abstract units of coefficients mapping normalized EEG voltages to kinematic parameters)

4. Discussion

4.1. Performance of Decoders

This study demonstrates for the first time the feasibility of extracting information of the kinematic parameters of walking from non-invasive electroencephalography in stroke survivors. Prior reported studies have only shown similar results in healthy animal and human subjects [26-28] or have focused their attention on decoding upper limb or non-walking-related leg movements in the stroke population [5-6, 8]. Decoding accuracies showed at worst moderate correlation between predicted and measured kinematics, and at best high correlation on par with the results from healthy subjects. Accuracies for one of four subjects were significantly lower, and the average accuracies might be higher than reported if this particular subject was regarded as an outlier.

Three decoding algorithms were used and compared in this study: the Wiener filter, and the unscented Kalman filter, and the 10^{th} order unscented Kalman filter. The Wiener filter was found to be both the most accurate and most efficient computationally in this offline analysis. Surprisingly, the 10^{th} order unscented Kalman filter had worse performance than the 1^{st} order filter despite using more past information to make predictions. It could be that ten was an unreasonably high order and led to overfitting, despite it being used most effectively in previous neural decoding work [37]. Because of its recursive algorithm, the Kalman filter has been used in a variety of applications for real-time prediction

applications and may not result in a loss of performance as the Wiener filter might for having less training data.

Moreover, principal component analysis was shown as an effective way to solve the problem of overfitting and dimensionality reduction for the EEG data with variables for each channel and time lag at every time sample. Other methods, such as sensor dropping and genetic algorithm, are more robust, yet computationally exhausting. PCA was quickly able to reduce dimensionality by a whole magnitude in most cases by finding the eigenvectors preserving the most variance, with a minimal dropoff in decoding accuracy. PCA did not help the overfitting in the case of the 10^{th} order unscented Kalman filter since it was applied to the EEG data prior to the decoding process.

Decoding accuracies were also reported to be higher for hip and knee joints over ankle joints and occasionally the paretic leg over the non-paretic leg. This is somewhat consistent in upper-limb decoding studies that found an inverse correlation between decoding accuracy and movement variability [40]. The ankle joints tend to have the widest swings during the gait cycle and the limited movement of the paretic leg may account for the reduced variability that increases decoding accuracy.

One surprising finding from the decoding analysis was the apparent equivalency in the decoding results from using EEG from only one hemisphere, either ipsilesional or

contralesional. These two conditions did not have any significant difference, but were significantly worse than using electrodes from both hemispheres. Because of the wide scalp coverage of EEG, it is possible that channels on the ipsilesional around the area of the lesions may still be healthy and contain sufficient information for decoding movement.

4.2. Power Spectral Density Analysis

In general, the results of the power spectral density analysis were too inconsistent and not significant enough to warrant conclusive results. This is most likely due to the small sample size and the wide variability of the effects of stroke in the subjects. Many of the results expected from previous literature were prevalent but not significant.

Nevertheless, one novel and perhaps significant finding from the PSD analysis was a possible downward shift in the mu-rhythm after stroke. The spectral signature for healthy subjects during walking show a sharp decline over the delta and theta bands and then a slight hump around 8-13 Hz. This hump was noted in all of the stroke subjects but at a lower range, between 5-10 Hz for S1, S2, and S3, and between 7-11 Hz for S4. The reported characteristics for the mu-band, such as suppression during movement [27, 39] and reduced ERD post-stroke [21], were also seen to some extent in this shifted range.

4.3. Correlates of Channel and Lag Weights

As in the PSD analysis, the results of finding decoding correlates across the EEG channels or the lags were mostly inconsistent and could be better determined with more well-defined subjects. This scalp map analysis may not necessarily be equivalent to mapping individual contributions of electrodes to decoding; the weights may more likely govern activation versus suppression of channels as they contribute positively or negatively towards a function representing kinematics. Nevertheless the consistent region of blue "suppression" in the right hemisphere is somewhat telling, given that all subjects were left paretic and had some amount of right hemispheric lesions. Previous studies in decoding walking from healthy EEG describe a "sparse but distributed cortical network", which may describe the maps generated here to some degree.

Given the small subject sample size, it is hard to draw concrete conclusions about the correlates of lag selection. Longer lags (>100 ms) likely contribute to motor planning, while more immediate lags are involved in execution. Including lags of a nonlinear scale give the model an opportunity to account for both.

4.3. Translatability to Rehabilitative Devices and Brain-Machine Interfaces

Our results demonstrate feasibility of decoding intended walking kinematics noninvasively from the brain of stroke survivors. A real-time implementation of this model could be used to drive a rehabilitative powered exoskeleton to aid in recovery,

reinforcing plasticity in lost neural circuits through continued use. Such exoskeletons are currently in development for non-neural control, such as the Rex system (Rex Bionics Ltd), and need only a reliable decoding algorithm for thought-driven walking (Figure 16). Other brain-machine interface (BMI) systems have attempted to provide user operation relying upon biofeedback or operant condition; a system that decodes limb kinematics is favorable since users can train with the BMI more intuitively [40-41]. A system that utilizes feedback and training in addition to kinematic decoding algorithms loosens the requirements on highly accurate decoders; training and feedback will help compensate for lower accuracy, and failed attempts of decoding intended movement may help the user learn to generate stronger and more consistent cortical signals [6]. BMI systems that uses noninvasive EEG signals also eliminates the risks and costs of invasive surgery for implanting electrodes within the skull.

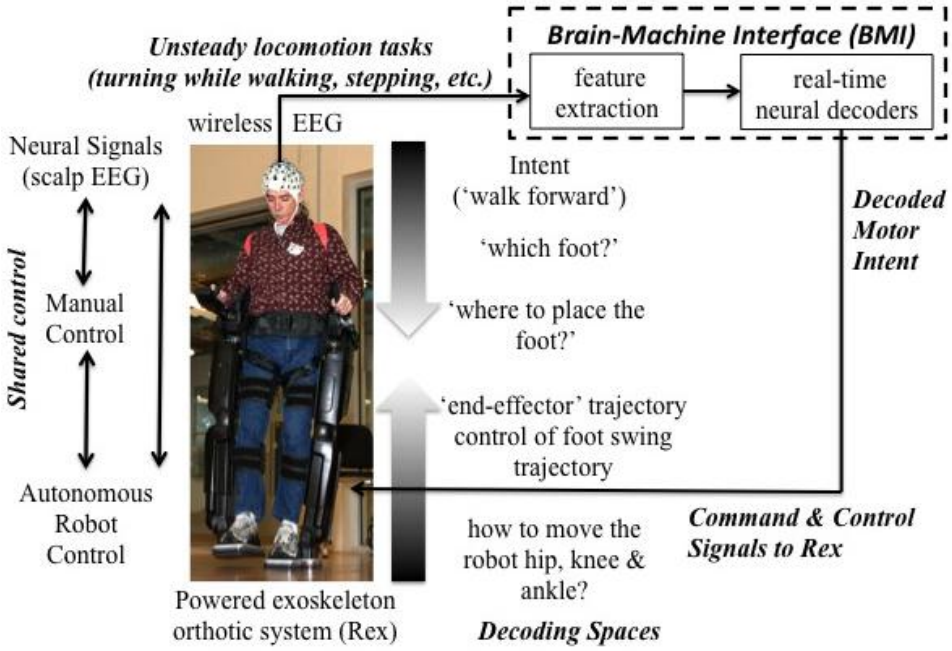

Figure 16. Flowchart for the implementation of an EEG-controlled powered walking exoskeleton (Rex, Rex Bionics Ltd) for restoration of gait. Courtesy of JL Contreras-Vidal (University of Houston)

4.4. Future Directions

As mentioned before, this study presents findings from the first attempts to decode walking kinematics from stroke survivors, and as such, there are numerous paths on which we can proceed to further advance our understanding of the problem and goals to solve them.

A number of the findings and results in the study were partially inconclusive due to variability, inconsistency, and lack of statistical significance, particularly for the PSD analysis and the mapping of the correlates of EEG channel and lag weights. Recruitment of more stroke patients with better-characterized stroke damage would give us a better sample size to reduce this variability. However, given the high variability among subjects in clinical populations such as that described in this study, it is imperative to treat each subject as an individual "within-subjects" case study.

This study can also be redone by decoding alternative sets of kinematic parameters. Here we solved for the *x*-, *y*-, and *z*-positions, the angular position, and the angular velocity for each of the six joints: left hip, left knee, left ankle, right hip, right knee, and right ankle. This was a rather high-dimensional problem, since thirty different variables were decoded for each condition, and these variables had some amount of correlation between them. A better understanding of biomechanics and human gait can identify the most essential parameters (possibly foot placement and timing, joint velocity) needed to reduce the degrees of freedom for this problem. Similarly, the problem could be simplified by

treating walking as a sequence of discrete states, rather than joints moving in continuous time. This also lends to the use of discrete state decoding algorithms such as classifiers and hidden Markov models that may be more computationally efficient as well.

Finally, the decoding algorithms need to be evaluated in real-time for any intent to be beneficial for stroke survivors with impaired gait. Real-time implementation allows for feedback that can improve decoder performance through training. With a real-time system, patients can use EEG to control walking in a powered exoskeleton (Figure 16) or possibly in a virtual avatar for training, where such practice would help the brain achieve plasticity through repeated use while reducing the patient's fatigue from physical therapy.

5. Conclusion

In conclusion, this feasibility study shows that the kinematics of walking could be decoded from the EEG of stroke patients with reasonable accuracy, and with best results on par with best decoding results from healthy subjects in prior studies. The spectral signature of the EEG saw potentially interesting differences between healthy and stroke, but in this study the differences were neither significant nor consistent. Similarly, determining the representation of walking in specific areas of the brain by identifying regional contributions also saw potentially interesting but statistically insignificant and inconsistent results. Recruitment of more subjects with more consistently characterized stroke lesions could reduce variability and provide better insight into some of the weaker observations noted here. Nevertheless, the prospects of using EEG to decode walking motion hold promise for future rehabilitative devices, and the field is still wide open for further exploration.

Appendix

A.1. IRB Approval Letter

Addendum Application Approval

To: Principal Investigator, Dr. Jose L. Contreras-Vidal, Kinesiology
Student, Mr. Kevin Nathan, Electrical and Computer Engineering

From: James M. Hagberg
IRB Co-Chair
University of Maryland College Park

Re: IRB Protocol: 10-0324 - Non-invasive neural decoding of walking from EEG signals

Approval Date: February 06, 2012

Expiration Date: June 02, 2012

Application: Addendum

Review Path: Expedited

The University of Maryland, College Park Institutional Review Board (IRB) Office approved your Addendum IRB Application. This transaction was approved in accordance with the University's IRB policies and procedures and 45 CFR 46, the Federal Policy for the Protection of Human Subjects. Please reference the above-cited IRB Protocol number in any future communications with our office regarding this research.

Recruitment/Consent: For research requiring written informed consent, the IRB-approved and stamped informed consent document will be sent via mail. The IRB approval expiration date has been stamped on the informed consent document. Please note that research participants must sign a stamped version of the informed consent form and receive a copy.

Continuing Review: If you intend to continue to collect data from human subjects or to analyze private, identifiable data collected from human subjects, beyond the expiration date of this protocol, you must submit a Renewal Application to the IRB Office 45 days prior to the expiration date.
If IRB Approval of your protocol expires, all human subject research activities including enrollment of new subjects, data collection and analysis of identifiable, private information must cease until the Renewal

Application is approved. If work on the human subject portion of your project is complete and you wish to close the protocol, please submit a Closure Report to irb@umd.edu.

Modifications: Any changes to the approved protocol must be approved by the IRB before the change is implemented, except when a change is necessary to eliminate an apparent immediate hazard to the subjects. If you would like to modify an approved protocol, please submit an Addendum request to the IRBOffice.

Unanticipated Problems Involving Risks: You must promptly report any unanticipated problems involving risks to subjects or others to the IRB Manager at301-405-0678 or jsmith@umresearch.umd.edu

Additional Information: Please contact the IRB Office at 301-405-4212 if you have any IRB-related questions or concerns. Email: irb@umd.edu

The UMCP IRB is organized and operated according to guidelines of the United States Office for Human Research Protections and the United States Code of Federal Regulations and operates under Federal Wide Assurance No. FWA00005856.

1204 Marie Mount Hall
College Park, MD 20742-5125
TEL 301.405.4212
FAX 301.314.1475
irb@umd.edu
http://www.umresearch.umd.edu/IRB

References

[1] Gibson C, Donnelly MA, Turner S (2009). One degree of separation: Paralysis and spinal cord injury in the United States. *Christopher and Dana Reeve Foundation*.

[2] Dobkin BH (2004). Strategies for stroke rehabilitation. *Lancet Neurol.*; 3, 528-536.

[3] Rosamond W, Flegal K, Friday G, Furie K, Go A, Greenlund K, Haase N, Ho M, Howard V, Kissela B, Kittner S, Lloyd-Jones D, McDermott M, Meigs J, Moy C, Nichol G, O'Donnell CJ, Roger V, Rumsfeld J, Sorlie P, Steinberger J, Thom T, Wasserthiel-Smoller S, Hong Y (2007). Heart disease and stroke statistics—2007 update: A report from the American Heart Association Statistics Committee and Stroke Statistics Subcommittee. Circulation; 155e69-e171.

[4] Gresham GE, Fitzpatrick TE, Wolf PA, McNamara PM, Kannel WB, Dawber TR (1975). Residual disability in survivors of stroke—The Framingham study. *N Engl J Med*; 293(19):954-956.

[5] Muralidharan A, Chae J, Taylor DM (2011). Early detection of hand movements from electroencephalograms for stroke therapy applications. *J Neural Eng*; 8(4):046003.

[6] Muralidharan A, Chae J, Taylor DM (2011). Extracting attempted hand movements from EEGs in people with complete hand paralysis following stroke. *Frontiers in Neuro;* 5(39).

[7] Forrester LW, Wheaton LA, Luft AR (2008). Exercise-mediated locomotor recovery and lower-limb neuroplasticity after stroke. *J of Rehab Research & Dev*; 45(2): 205-220.

[8] Bundy DT, Wronkiewicz M, Sharma M, Moran DW, Corbetta M, Leuthardt EC (2012). Using ipsilateral motor signals in the unaffected cerebral hemisphere as a signal platform for brain-computer interfaces in hemiplegic stroke survivors. *J Neural Eng.*; 9(3):035011.

[9] Taylor DM, Tillery SI, Schwartz AB (2008). Direct cortical control of 3d neuroprosthetic devices. *Science*; 296: 1829-1832.

[10] Wolpaw JR, McFarland DJ (2004). Control of a two-dimensional movement signal by a noninvasive brain-computer interface in humans. *Proc. Natl Acad. Sci. USA*; 101: 17849-17854.

[11] Rouse AG, Moran DW (2009). Neural adaptation of epidural electrocorticographic (EECog) signals during closed-loop brain computer interface (BCI) tasks. *Conf. Proc. IEEE Eng. Med. Biol. Soc.*; vol 2009: 5514-5517.

[12] Wisneski KJ, Anderson N, Schalk G, Smyth M, Moran D, Leuthardt EC (2008). Unique cortical physiology associated with ipsilateral hand movements and neuroprosthetic implications. *Stroke*; 39: 3351-3359.

[13] Enzinger C, Johansen-Berg H, Dawes H, Bogdanovic M, Collett J, Guy C, Ropele S, Kischka U, Wade D, Fazekas F, Matthews P (2008). Functional MRI correlates of lower limb function in stroke victims with gait impairment. *Stroke*; 39(5): 1507-1513.

[14] Ward NS, Brown MM, Thompson AJ, Frackowiak RSK (2004). The influence of time after stroke on brain activations during a motor task. *Ann Neurol.*; 55:829-834.

[15] Johanseng-Berg H, Dawes H, Guy C, Smith SM, Wade DT, Matthews PM (2002). Correlation between motor improvements and altered fMRI activity after rehabilitative therapy. *Brain*; 125:2731-2742.

[16] Luft AR, Waller S, Forrester L, Smith GV, Whitall J, Macko RF, Schulz JB, Hanley DF (2004). Lesion location alters brain activation in chronically impaired stroke survivors. *NeuroImage*; 21: 924-935.

[17] Cao Y, D'Olhaberriague L, Vikingstad EM, Levine SR, Welch KM (1998). Pilot study of functional MRI to assess cerebral activation of motor function after poststroke hemiparesis. *Stroke*; 29: 112-122.

[18] Cramer SC, Nelles G, Benson RR, Kapla JD, Parker RA, Kwong KK, Kennedy DN, Finklestein SP, Rosen BR (1997). A functional MRI study of subjects recovered from hemiparetic stroke. *Stroke*; 28: 2518-2527.

[19] Rossini PM, Caltagirone C, Castriota-Scanderbeg A, Cicinelli P, Del Gratta C, Demartin M, Pizzella V, Traversa R, Romani GL (1998). Hand motor cortical area reorganization in stroke: a study with fMRI, MEG, and TCS maps. *NeuroReport*; 9: 2141-2146.

[20] Luft AR, Macko RF, Forrester LW, Villagra F, Ivey F, Sorkin JD, Whitall J, McCombe-Waller S, Katzel L, Goldberg AP, Hanley DF (2008). Treadmill exercise activates subcortical neural networks and improves walking after stroke: a randomized controlled trial. *Stroke*; 39: 3341-3350.

[21] Stepien M, Conradi J, Waterstaat G, Hohlefeld FF, Curio G, Nikulin VV (2010). Event-related desynchronizaiton of sensorimotor EEG rhythms in hemiparetic patients with acute stroke. *Neuroscience Letters*; 488: 17-21.

[22] Antelis JM, Montesano L, Ramos-Murguialday A, Birbaumer N, Minguez J (2012). Continuous decoding of intention to move from contralesional hemisphere brain oscillations in severely affected chronic stroke patients. *34th Annual International Conference of the IEEE Engineering in Medicine and Biology Society (EMBS)*.

[23] Miller KJ, Abel TJ, Hebb AO, Ojemann JG (2011). Reorganization of large-scale physiology in hand motor cortex following hemispheric stroke. *Neurology*; 76: 927-929.

[24] Sarnthein J, Morel A, Stein AV, Jeanmonod D (2003). Thalamic theta field potentials and EEG: high thalamocortical coherence in patients with neurogenic pain, epilepsy and movement disorders. *Thalams Reat Syst*; 2: 231-238.

[25] Caporale N, Dan Y(2008). Spike timing-dependent plasticity: a Hebbian learning rule. *Annu Rev. Neurosci*; 31: 25-46.

[26] Fitzsimmons NA, Lebedev MA, Peikon ID, Nicolelis MAL (2009). Extracting kinematic parameters for monkey bipedal walking from cortical neuronal ensemble activity. *Front. Integr Neurosci.*; 3(3).

[27] Presacco A, Goodman R, Forrester L, Contreras-Vidal JL (2011). Neural decoding of treadmill walking from non-invasive electroencephalographic (EEG) signals. *J Neurophysiol*; 106: 1875-1887.

[28] Presacco A, Forrester LW, Contreras-Vidal JL (2012). Decoding intra-limb and inter-limb kinematics during treadmill walking from scalp electroencephalographic (EEG) signals. *IEEE Transactions on Neural Systems and Rehab Engr.*; 20(2): 212-219.

[29] Lebedev MA, Nicolelis MA (2006). Brain-machine interfaces: past, present and future. *Trends Neurosci*; 29: 536-546.

[30] Yogev-Seligmann G, Hausdorff JM, Giladi N (2008). The role of executive function and attention in gait. *Mov Disord*; 23: 329-342.

[31] Jasper HH (1958). The ten-twenty electrode system of the International Federation. *Electroencephalogr Clin Neurophysiol*; 10: 371-375.

[32] Percival DB, Walden AT (1993). Spectral analysis for physical applications: multitaper and conventional univariate techniques. *Cambridge University Press*.

[33] Thompson DJ (1982). Spectrum estimation and harmonic analysis. *Proceedings of the IEEE*; 70: 1055-1096.

[34] Goncharova II, McFarland DJ, Vaughan JR, Wolpaw JR (2003). EMG contamination of EEG: spectral and topographical characteristics. *Clin Neurophysiol*; 114: 1580-1593.

[35] Haykin S (2002). Adaptive Filter Theory. Upper Saddle River, NJ: Prentice Hall.

[36] Haykin S (2001). Kalman Filtering and Neural Networks. New York, NY: John Wiley & Sons, Inc.

[37] Li Z, O'Doherty JE, Hanson TL, Lebedev MA, Henriquez CS, Nicolelis MAL (2009). Unscented Kalman filter for brain-machine interfaces. *PLoS One*; 4(7): e6243.

[38] Delorme A, Makeig S (2004). EEGLAB: an open source toolbox for analysis of single-trial EEG dynamics including independent component analysis. *J Neurosci Methods*; 134: 9-21.

[39] Pfurtscheller G, Brunner C, Schlogl A, Lopes da Silva FH (2006). Mu rhythm (de)synchronization and EEG single-trial classification of different motor imagery tasks. *NeuroImage*; 31: 153-159.

[40] Bradberry TJ, Gentili RJ, Contreras-Vidal JL (2010). Reconstructing three-dimensional hand movements from noninvasive electroencephalographic signals. *J Neurosci*; 30: 3432-3437.

[41] Acharya S, Fifer MS, Benz HL, Crone NE, Thakor NV (2010). Electrocorticographic amplitude predicts finger positions during slow grasping motions of the hand. *J Neural Engr*; 7(4): 046002.